ACS Sustainable Chemistry & Engineering

Research Article

pubs.acs.org/journal/ascecg

Liquid Crystalline Behaviors of Chitin Nanocrystals and Their Reinforcing Effect on Natural Rubber

Yongwang Liu,[†] Mingxian Liu,*[,†] Shuyan Yang,[‡] Binghong Luo,[†] and Changren Zhou[†]

[†]Department of Materials Science and Engineering, Jinan University, Guangzhou 510632, People's Republic of China

[‡]Dongguan Cleaner Production Center, Dongguan University of Technology, Dongguan 523808, People's Republic of China

ABSTRACT: Chitin nanocrystals (CNCs), rod-like crystalline nanoparticles from natural sources, show high aspect ratio, high modulus, and excellent reinforcing ability toward polymers. In this study, CNCs aqueous dispersions were first prepared by acid hydrolysis of raw chitin. The resulting dispersion was investigated by polarized optical microscopy and rheometry at different CNCs concentrations. A nematic liquid crystals phenomenon with increasing solid concentration is found in the CNCs dispersion. When the concentration of CNCs dispersion is beyond 5 wt %, the dispersion forms liquid crystal phase. CNCs dispersions were then compounded with natural rubber (NR) latex to prepare NR/CNCs composites. CNCs are evenly dispersed in NR matrix, which can effectively enhance the mechanical properties and thermal stability of rubber. The tensile strength of NR/CNCs composite containing 10 wt % CNCs is 5.75 MPa, which is 6.25 multiples of pure NR. Also, the tear strength, storage modulus, and thermal decomposition temperature of the composites increase with increasing CNCs loading. The improvement of NR properties is caused by the uniformly dispersed CNCs and the good interfacial interactions between CNCs and rubber molecular chains. NR/CNCs composites show many advantages such as light color, lightweight, and high performance over the traditional carbon black-filled rubber.

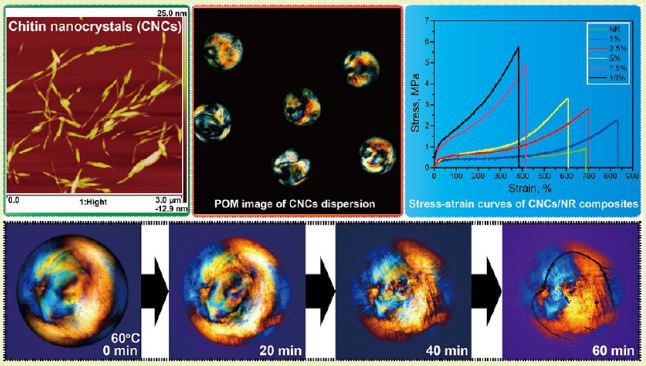

KEYWORDS: *Chitin nanocrystals, Liquid crystalline, Nature rubber, Composite, Mechanical property*

INTRODUCTIONS

Chitin, a long-chain polymer of *N*-acetylglucosamine, is present in many animals and plants throughout the natural world.[1−3] Chitin nanocrystals (CNCs), originating from acid hydrolysis of crude chitin, are crystalline and positively charged rod-like particles.[4,5] CNCs show a good dispersion in water, high aspect ratio, high modulus, and excellent reinforcing ability toward polymers.[6,7] The rod-like structure of CNCs usually has a width range of 10−50 nm and a length range of 150−200 nm, which results in a high aspect ratio. The elastic modulus of CNCs is ∼150 GPa, which can provide a strong reinforcement effect on polymers.[8] For example, CNCs are employed as reinforcing materials for polymer hydrogels, and CNCs act as a physical cross-linker through hydrogen bond interactions with polymer chains in the composite systems.[8,9] CNCs-incorporated polymer hydrogels not only exhibit improved mechanical properties but also show good biocompatibility.[10,11] In addition, the thermal stability and biological ability of polymer/CNCs composites can also be improved by CNCs.[12,13] For instance, poly(L-lactide)-grafted CNCs can simultaneously improve mechanical properties, crystallinity, and cellular compatibility of poly(L-lactide) matrix.[14−16] CNCs were also incorporated into the rubber matrix as reinforcement materials, and the results demonstrate that the processing methods and surface modification of CNCs had a significant effect on the properties of composites.[17−19] Previously, we used the CNCs as nanofiller to reinforce carboxylated styrene−butadiene rubber (x-SBR) through solution mixing. A significant improvement of the mechanical performance and water-triggered modulus changes of x-SBR was achieved by CNCs.[20,21] However, the processing−structure−performance relationships of the rubber/CNCs composites are not fully understood as their counterparts of cellulose nanocrystals.[22−24] Also, CNCs were added to chitosan to increase the mechanical behavior and cell adhesion properties.[25−27] CNCs-reinforced polymer composites combine the comprehensive advantages including high strength, lightweight, light color, biodegradability, and biocompatibility. However, the critical factors determining the performance of composites are agglomerates and lack of interfacial interactions, which weaken the load transfer from the polymer matrix to the CNCs.

The dispersion and assembly behavior of CNCs are important for their application in polymer nanocomposites. In particular, owing to their high aspect ratios and the interactions among nanocrystals, CNCs dispersions can form liquid crystalline phases, just like those observed in carbon

Received: July 29, 2017
Revised: October 1, 2017
Published: November 1, 2017

DOI: 10.1021/acssuschemeng.7b02586
ACS Sustainable Chem. Eng. 2018, 6, 325−336

nanotubes (CNTs), graphene oxide (GO), clay minerals, and cellulose nanocrystals. The liquid crystal behavior of the nanoparticles is affected not only by the dispersion concentration but also by the pH and temperature.[28] For example, cellulose nanocrystals can produce stable aqueous suspension that exhibit cholesteric liquid-crystalline behavior at higher concentrations.[29] The hierarchical cholesteric architectures can be prepared via self-assembly of cellulose nanocrystals in shrinking, micrometer-sized aqueous droplets.[30] Halloysite nanotubes (HNTs), a natural nanoclay with unique tubular structure, also showed liquid crystalline behavior at an aqueous dispersion concentration higher than 1 wt %.[31] GOs, flaky nanoparticles, also have liquid crystalline behavior.[32] The isotropic−nematic phase transition of GO aqueous dispersion appears at a mass concentration of ∼0.025%, and a stable nematic phase occurs at ∼0.5%.[33] There has been an enormous amount of research on the liquid crystal of cellulose[29,34−36] but few reports on chitin liquid crystal.[37−44] Revol et al. found that CNCs aqueous suspension can display chiral nematic order, and dried CNCs film showed helicoid organization features like chitin microfibrils in the cuticle of arthropods as early as 1993.[37] However, the polarized light phenomenon of the nematic phase of CNCs and the formation of assembled CNCs structure in oil phase formation have not been systematically studied. The research on the liquid crystal formation conditions of CNCs is critical for guiding its application in various areas, like biomedical materials[45,46] and orderly functional material,[47] owing to the many unique characteristics of CNCs.

It is necessary to compare the CNCs with well-developed cellulose nanocrystals. Both cellulose nanocrystals and CNCs are renewable natural nanocrystals derived from polysaccharides. However, the sources of the two polymers are different. Cellulose is largely found in plants, which is considered to be the oldest component of cell walls of plants, algae, and in some bacteria. In contrast, chitin is mainly found in the exoskeleton of animals such as mollusks, crab, and lobster. In addition, the chemical formula of the two polymers is different. Cellulose has a formula of $(C_6H_{10}O_5)_n$, while chitin has the formula of $(C_8H_{13}O_5N)_n$, which contains amino acids and an acetyl functional group (*N*-aceytlglucosamine). Lastly, the surface charge character of these two nanocrystals is different. CNCs are positively charged, while cellulose nanocrystals are negatively charged. Chitin is of strategic significance owing to its fascinating functionalities as immunoregulation, anti-inflammatory, antithrombogenesis, and cell viability.[5] Moreover, the large aspect ratio, high Young's modulus, and biodegradability make CNCs excellent candidates as nanoreinforcements in polymer composites. The use of CNCs as nanofillers for polymers opens an alternative way for utilization of animal polysaccharides.

In this study, the liquid crystalline behavior and sol−gel transition behavior of CNCs aqueous dispersions are examined by polarized optical microscopy (POM), macroscopic observation, and rheometry. The observation of CNCs droplet shrinkage upon heating process at 60 °C was conducted by POM for monitoring of the pitch evolution as a function of the water content. Afterward, CNCs aqueous dispersion is added to natural rubber (NR) latex to form composite films via solution mixing and casting drying method. The formation of a network structure via self-assembly of CNCs in rubber matrix contributes to the enhancement of the mechanical performance of the composites. The interfacial interactions, morphology, and mechanical properties were investigated by various techniques. The properties improvement of the NR composite is found by the addition of CNCs, which is related to the evenly dispersed CNCs and the interfacial interactions. The prepared NR/CNCs composites show many advantages such as light color, lightweight, and high performance over the traditional carbon black-filled rubber. This work provides a new perspective for converting renewable chitin sources into high-performance polymer composites and will promote the research and application on macroscopic assembly of CNCs.

EXPERIMENTAL SECTION

Materials. Chitin (practical grade) was obtained from Shanghai Aladdin Bio-Chem Technology Co., Ltd. Natural rubber (NR) latex (without addition of vulcanizing agent) was purchased from Dongguan Tunchang Xinyuan Rubber Trading Co. Ltd. (China). The percentage of dry rubber content of the latex was about 60. Hydrochloride acid (HCl) and other chemicals were of analytical grade. Ultrapure water (resistivity > 18.2 MΩ.cm) was prepared with a Millipore purification apparatus.

Preparation of Chitin Nanocrystals (CNCs) and CNCs Dispersions. The CNCs were prepared by the acid hydrolysis method according to ref 17. Typically, raw chitin was mechanically mixed with 3 N HCl at a 30 $mL{\cdot}g^{-1}$ ratio for 90 min at 104 °C. Afterward, the dispersions were centrifuged for 10 min at 4000 rpm and washed by ultrapure water three times. During this process excessive acid and the amorphous phase were almost removed. The dispersions were then transferred to dialysis bags and dialyzed in flowing water for 24 h. Finally, the CNCs powders were obtained by freeze drying. To obtain a uniform dispersion of different concentrations of CNCs dispersions, the dispersions were ultrasonically treated by a JY99-IIDN ultrasonic cell disruptor (NingBo Scientz Biotechnology Co., Ltd., China) at 570 W for 1 h.

Fabrication of NR/CNCs Composite Films. NR/CNCs composite films were prepared by the solution-casting method. Before the process of blending with NR latex, 0.06, 0.15, 0.3, 0.45, and 0.6 g of CNCs was added into 20 mL of water, and then the mixtures were ultrasonically treated for 1 h at 570 W to get different concentrations of CNCs dispersion. Meanwhile, 10 g of NR latex (solid content of the latex is 60%) was diluted using 20 mL of water. Afterward, CNCs dispersions were added to the uniform NR latex with stirring for at least 5 h to obtain a homogeneous mixture. The NR/CNCs composite films were obtained by oven drying at 60 °C for 16 h in a square PTFE mold (10 cm × 10 cm).

Characterization. *Atomic Force Microscopy (AFM).* CNCs were observed by a multimode AFM with a NanoScope IIIa controller (Veeco Instruments Inc.) with Tap 150-Al-G silicon AFM probes. The experiment was conducted in ScanAsyst mode at 256 × 256 pixels at 25 °C. The sample for AFM analysis was prepared by dropping of the 0.01 wt % CNCs dispersion on a clean mica plate and dried at room temperature.

ξ-Potential Analysis. The ξ-potential of CNCs aqueous dispersions was measured using a Zetasizer (Nano ZS, Malvern Instruments Ltd., UK). The concentration of the dispersion was 1×10^{-3} wt %. Before determination, the samples were subjected to ultrasonic treatment for 1 h at 570 W.

Transmission Electron Microscopy (TEM). A 0.02 wt % of CNCs aqueous dispersions was dropped and dried on amorphous carbon film-supported copper mesh grid. The samples were observed using Tecnai Philips 10 TEM at an accelerating voltage of 100 kV.

Scanning Electron Microscopy (SEM). A 0.02 wt % of CNCs aqueous dispersions was dropped in glass pieces and dried naturally; after spray treatment, the samples were observed on a ZEISS Ultra 55 SEM. The NR/CNCs composite films were broken in liquid nitrogen, and then the cryofractured surface of the composites films was observed by SEM. Before observation, a thin gold layer was sprayed on the sample surfaces.

Polarized Optical Micrographs (POM). Different CNCs aqueous dispersions in capillary tubes were observed using the ZEISS SteREO Discovery V20 (Germany) under crossed polarizers. Drops of CNCs

DOI: 10.1021/acssuschemeng.7b02586
ACS Sustainable Chem. Eng. 2018, 6, 325−336

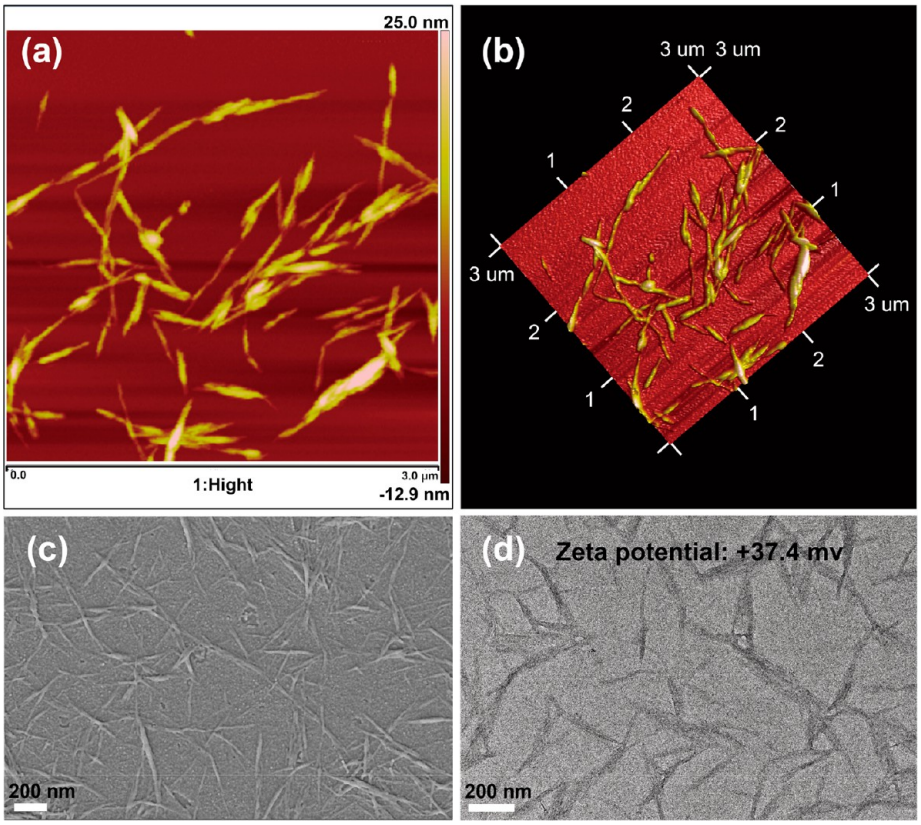

Figure 1. AFM height image (a) and 3D image (b) of CNCs; SEM image of CNCs (c); high-resolution TEM image of CNCs and zeta potential of CNCs aqueous dispersion (d).

dispersion were injected into a continuous phase comprised of silicone oil via a pipet gun (diameter of the tips is 0.45 mm). The POM photos of CNCs droplet were taken by an Olympus BX53M.

Rheology. The dynamic viscosity of the CNCs dispersion was determined by a rotational rheometer (Kinexus pro+, Malvern Instruments, Malvern, UK.) at 25 °C at a shear rate of 1−100 s^{-1}. The testing was conducted using parallel plates mode with a plate diameter of 40 mm and gap between the two parallel plates of 0.05 mm. A dynamic frequency sweep test from 0.1 to 100 rad/s at a fixed strain of 0.5% was performed to measure the dynamic storage modulus (G') and loss modulus (G'') of each CNCs dispersion.

Fourier Transforms Infrared Spectroscopy (FTIR). FTIR spectra of neat NR and NR composites were measured using attenuated total reflection (ATR) in a NICOLET iS10 FT-IR Spectrometer. The signals of 32 scans were averaged from 4000 to 400 cm^{-1} at a wavenumber resolution of 2 cm^{-1}.

X-ray Diffraction (XRD). XRD patterns of CNCs, neat NR, and NR/CNCs composite films were determined using an X-ray diffractometer (Rigaku, Miniflex600, Japan) with Cu Kα radiation (λ = 0.154178 nm at 40 kV and 40 mA). The testing was conducted with a scanning rate of 5°/min from 3° to 50°.

Mechanical Properties Determination. Dumbbell-shaped rubber samples with width × thickness of 6 mm × 0.3 mm were prepared for tensile testing. A universal testing machine (UTM-Q422, Chende Jinjian Testing Instrument Co., Ltd., China) was used to determine the tensile properties at a strain rate of 50 mm/min. The modulus at strain of 100%, 300%, and 500% was the tensile stress at a strain of 100%, 300%, and 500%, respectively. The tear test adopted the national standard (GT/T 529-1999) of the right angle sample. The cyclic tensile test was conducted at a strain rate of 50 mm/min to 100%, 200%, 300%, 400%, 500%, and 600% strain.

Dynamic Mechanical Analysis (DMA). DMA experiment was carried out by NETZSCH DMA 242 in a tensile mode at an oscillation frequency of 1.0 Hz. The temperature ranged from −100 to 60 °C with a heating rate of 5 °C/min. The experiments were conducted under nitrogen atmosphere.

Differential Scanning Calorimetry (DSC). DSC thermal analysis was conducted by a TAQ20 analyzer (TA Instruments, USA) using nitrogen as purging gas. The temperature range was from −90 to 60 °C with a heating rate of 10 °C/min. To evaluate the amount of immobilized rubber around the particles in the composite, the value of the heat capacity step ΔC_{pn}, which corresponds to the internal degree of freedom in molecular motion, was calculated by DSC result. From the ΔC_{pn} value, the mass percent of the immobilized polymer layer χ_{im} could be obtained. ΔC_{pn} and χ_{im} were calculated as follows

$$\Delta C_{pn} = \Delta C_p/(1 - w) \quad (1)$$

$$\chi_{im} = (\Delta C_{p0} - \Delta C_{pn})/\Delta C_{p0} \quad (2)$$

Here, ΔC_p is the heat capacity jump at T_g (from −70 to −60 °C in the present systems) which can be calculated by TAQ20 analyzer software, w is the mass percent of filler, ΔC_{pn} is normalized to the polymer weight fraction, and ΔC_{p0} is the heat capacity jump around T_g of neat polymer.

Thermogravimetric Analyzer (TGA). TGA curves of neat NR and NR/CNCs composite were tested using the NETZSCHTG 209 F3 Tarsus under a nitrogen atmosphere from room temperature to 600 °C at a heating rate of 10 °C/min.

RESULTS AND DISCUSSION

Characterization of CNCs. Ultrasound treatment of bundled chitin microfiber-derived acidolysis product results in a stable colloidal suspension of chitin crystalline at the nanoscale. The morphology and size of CNCs are first investigated by microscopy and DLS. Figure 1a and 1b shows the AFM height image and 3D image of CNCs. CNCs are in the form of rod-like microstructures and dispersed evenly. The

DOI: 10.1021/acssuschemeng.7b02586
ACS Sustainable Chem. Eng. 2018, 6, 325−336

average width and length of CNCs is ~50 nm and 200−1000 nm, which gives an aspect ratio of 4−20.[48] SEM and TEM images of CNCs also confirm the morphology of the CNCs. Figure 1c shows SEM photos of CNCs, which agrees with the AFM result. CNCs exhibit rod-like structure, and some of them form a weak bundle state. In the TEM photos shown in Figure 1d, CNCs are also uniformly dispersed with a width of ~50 nm and length between 200 and 1000 nm. The CNCs dispersion is highly positively charged with ζ-potential values of +37.4 mV, which proves the stability mechanism of CNCs dispersion. In total, the high aspect ratio, nanorod-like structure, and high dispersibility of CNCs endows promising applications in polymer composites.

Liquid Crystalline Behaviors and Rheological Properties of CNCs Dispersions. Figure 2a show photos of the

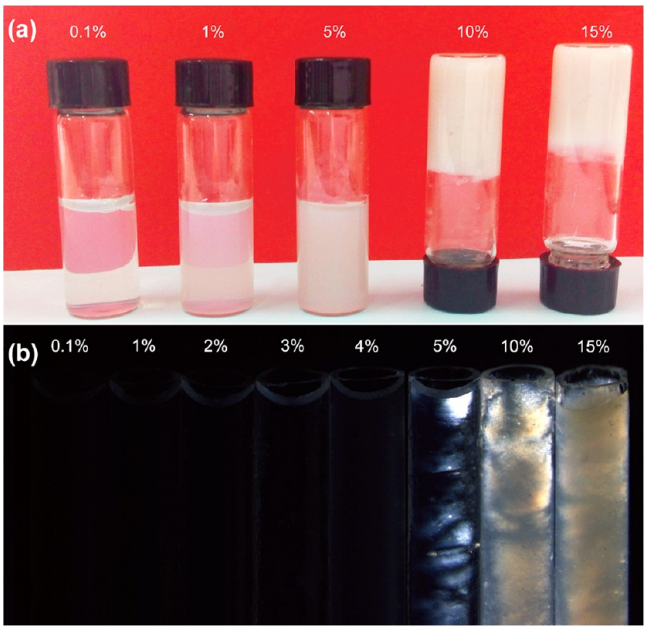

Figure 2. Images of different concentrations of CNCs dispersion (a); POM images of different concentrations of CNCs dispersion in the capillary (b).

CNCs aqueous dispersions after ultrasonic treatment for 1 h. The CNCs dispersions at relatively low concentration are uniform without sediments, which suggests the high dispersion stability of CNCs in aqueous media. When the concentration of CNCs dispersion is more than 10 wt %, CNCs dispersions cannot flow when pouring out the sample. Thus, the sol−gel transition of CNCs aqueous dispersions occurs upon increasing the CNCs concentration, which agrees with the previously reported HNTs aqueous dispersion systems.[31] The zeta-potential value indicates the stability of nanoparticle dispersions. The higher the magnitude of the zeta potential, the greater the degree of electrostatic repulsion among the charged particles. The increased electrostatic repulsion confers the stability of a dispersion and prevents aggregation of nanoparticles.

Due to the sufficient dispersibility and stability of CNCs aqueous dispersion, liquid crystalline phase can be obtained in certain conditions. CNCs can form a liquid crystalline phase that exhibits intense color under a polarizing microscope, which has been confirmed by Tzoumaki et al.[49] The polarized optical micrographs of CNCs aqueous dispersions in capillary tubes are displayed in Figure 2b. From the image, CNCs dispersion is almost transparent in the polarizing microscope at a concentration of less than 5 wt %, indicating its isotropic phase. When the concentration of CNCs dispersion is beyond 5 wt %, it begins to have prominent optical birefringence. With the increase of the CNCs concentration, the nematic schlieren texture consisting of dark and bright brushes is more obvious. This demonstrates that CNCs can form liquid crystal phase when the concentration is above 5%.

The formation of the liquid crystal phase of CNCs is further investigated using the POM technique. The evolved birefringence between analyzer and polarizer is commonly considered as direct evidence for the formation of lyotropic liquid crystalline phase.[31] A series of POM images of CNCs dispersions is displayed in Figure 3. When the CNCs concentration is 1 wt % or lower, the dispersion exhibits an isotropic state without birefringence under polarized light (Figure 3a). The evolution of birefringence domains confirms the isotropic−nematic phase transition which begins at a concentration of 5 wt %. With increasing CNCs concentration, more compact optical textures and stronger birefringence are emerging. When CNCs concentration is beyond 10 wt %, the dispersion exhibits birefringence with intense colors. This demonstrates the successful formation of the liquid crystal phase. A similar phase transition was reported in a previous study on GO[50] and montmorillonite.[51]

The droplets of CNCs dispersion (~650 μm in diameter) in the oil phase also exhibit interesting hierarchical cholesteric architectures (Figure 3b−e). From the droplet image of CNCs as imaged in transmission mode (Figure 3b), a round shape with a uniform diameter can be formed in the silicone oil medium. Interestingly, isotropic−nematic phase transition of CNCs dispersion begins at a concentration of 5 wt % under polarized light. The droplets at a concentration of 10 wt % completely form the liquid crystal phase with beautiful birefringence color. The formation of the cholesteric phase of CNCs is due to the self-assembly of the nanoparticle in oil medium, resulting in concentric ordering within the droplet. In high-magnification POM photos (Figure 3e) a local lamellar ordering of CNCs can be observed in the droplet. The hierarchical self-assembly of cellulose nanocrystals into cholesteric architectures was also reported in a confined geometry using oil as medium.[30]

POM images of CNCs dispersion at a concentration of 10 wt % droplets in oil were imaged under cross-polarizers (right) and with a first-order tint plate (left) (Figure 4). Different from the previously reported cellulose nanocrystals which gives rise to a pronounced Maltese cross-like pattern in the oil phase under crossed polarizers, intense birefringence color is found in the CNCs droplet. This may arise from the difference in dimension of the two droplets. In the present system the droplet diameter of CNCs dispersion is ~650 μm, while the cellulose nanocrystals droplet is 140 μm in diameter. The dimensional droplet is related to the viscosity of the dispersion, oil property, and pipet tips diameter. At such a high concentration, the CNCs suspension is highly viscous and almost entirely in a liquid crystalline phase. This droplet remains trapped in disordered anisotropic state without any particular reordering of the structure. The droplets in the oil can maintain the initial shape and interference color pattern unchanged for a long time (several hours).

Figure 5 shows the POM images of the entire evaporation process of the CNCs droplets in oil heated at 60 °C. With

DOI: 10.1021/acssuschemeng.7b02586
ACS Sustainable Chem. Eng. 2018, 6, 325−336

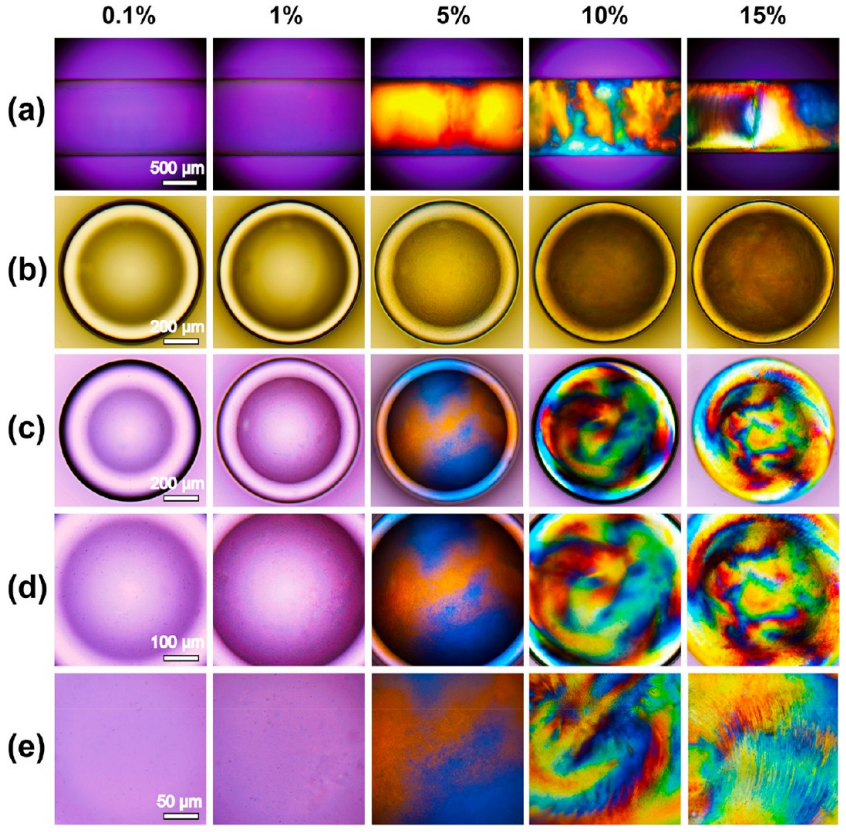

Figure 3. POM images of different concentrations of CNCs dispersion in the capillary (a); ordinary light images of the droplets of CNCs dispersions in silicone oil with different concentration (b); POM images of the droplets of different concentrations of CNCs dispersion in silicone oil with different magnifications (c–e).

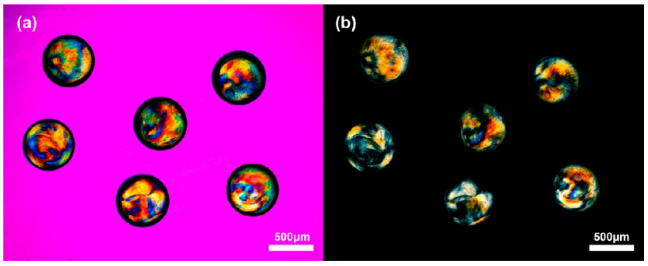

Figure 4. POM images of droplets containing a 10 wt % CNCs dispersion with addition of the sensitive tint plate insertion (a); without adding the sensitive tint plate insertion (b).

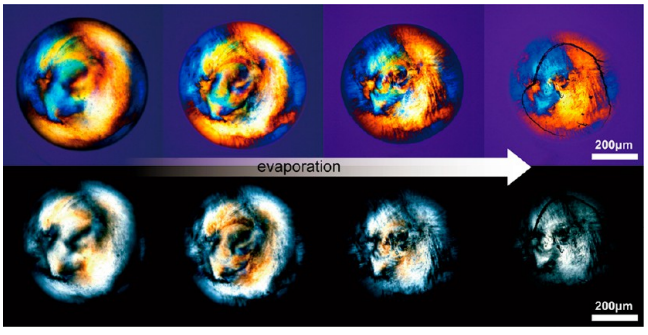

Figure 5. POM images of droplets initially containing a 10 wt % CNCs dispersion (left). Initial interference color pattern is retained upon evaporation to form dry microparticles (right).

increasing time the volume of droplets shrinks gradually. Finally, the water in the droplets is evaporated completely. Upon loss of water, the initial interference color pattern of CNCs droplet is retained even upon final drying. The interference color pattern is related to the ordering of the nanocrystal by the self-assembly process in oil. The ordering is preserved during the final stages of water loss from the droplet, but the bucking of the droplet occurs due to the loss of water. This can be attributed to the interplay between increasing Laplace pressure and the resistance to isotropic compression of the solidified CNC shell of the microdroplet during loss of water.[30] The organization of the CNCs into an ordered structure is critical for forming macroassembled CNCs architecture with tuned structure and ordered morphology.

The relationship between the shear viscosity and the shear rate at 25 °C of CNCs dispersions at different concentrations is presented in Figure 6a. The rheological properties of all CNCs dispersions show decreased viscosity upon shear, which suggests a typical shear-thinning behavior owing to the destruction of the CNCs network. When the concentration of CNCs dispersion is more than 10 wt %, the dispersion turns into a gel-like state at static state. On further increasing the concentration of CNCs to 15 wt %, the steady shear viscosity curve of the gel is almost overlapped with the 10 wt % samples.

The formation of 3D networks of nanoparticles via physical interactions (van der Waals, hydrogen bonds, and electrostatic interactions) can be studied by rheological methods.[41,52] The dependences of storage modulus (G') and loss modulus (G'') on the angular frequency (ω) of CNCs aqueous dispersions are plotted in Figure 6b. The CNCs dispersions with 5, 10, and 15

DOI: 10.1021/acssuschemeng.7b02586
ACS Sustainable Chem. Eng. 2018, 6, 325–336

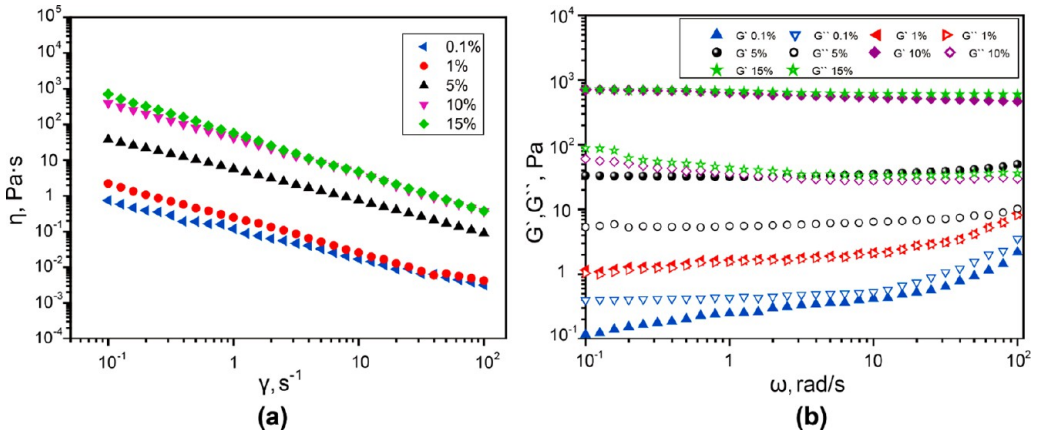

Figure 6. Dynamic viscosity of different concentrations of CNCs dispersion (a); storage modulus and loss modulus of different concentrations of CNCs dispersion (b).

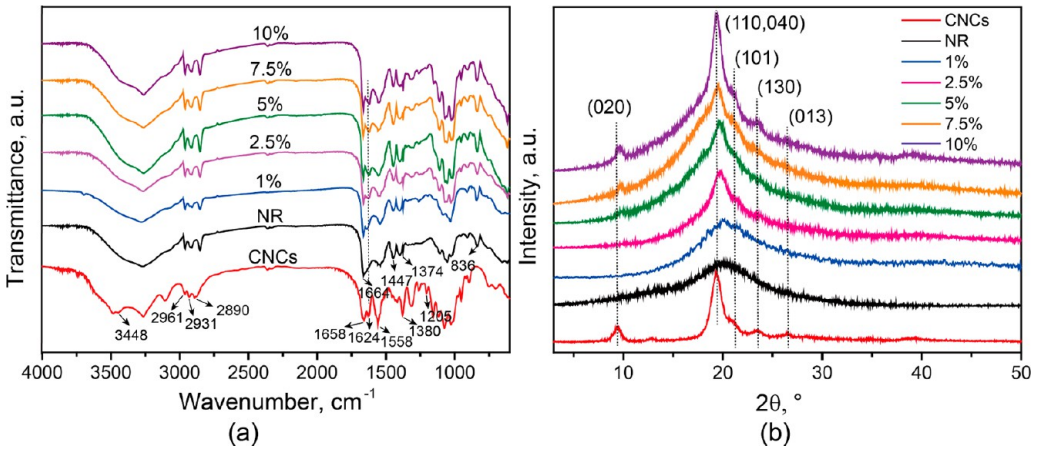

Figure 7. FTIR spectra of NR, CNCs, and NR/CNCs composites (a); XRD patterns of NR, CNCs, and NR/CNCs composites (b).

wt % concentration behave elastically just like an ideal gel. G' of the CNCs dispersions are almost independent of frequency, and G' is much higher than G'', whereas for the CNCs dispersion with a concentration of 0.1 wt % the G' is lower than G'' in the whole frequency range (like a liquid-like behavior). The G' and G'' of the CNCs dispersion with 1 wt % concentration almost overlap with each other in the tested frequency range. Thus, the liquid-like to solid-like behavior transition of CNCs dispersions occurs at 1 wt % concentration. The increase in CNCs aqueous dispersions concentration leads to a transformation from a viscous fluid to an elastic gel, which is consistent with the observation above.

Structure of the NR/CNCs Composites. The IR technique was first used to analyze the components of the NR/CNCs composites (Figure 7a). In the spectrum of CNCs, it exhibits typical absorbance peaks around 3448 (O−H and N−H stretching vibrations), 1658 (C═O stretching in −CONH−), 1624 (intermolecular hydrogen bonded to C═O), 1556 (amide II), and 2961−2931−2890−1380−1205 cm^{-1} (C−H bonds). These peaks are consistent with the characteristic peaks of *a*-chitin.[17,53] The spectra of pure NR show peaks at 1664 cm^{-1} assigned to the C═C stretching vibration, 1447 and 1374 cm^{-1} assigned to the deformation of C−H_2, and 836 cm^{-1} assigned to the bending of C−H. The IR peaks of the neat NR sample are consistent with the spectra shown in the previous literature.[54,55] After incorporation of CNCs, the composites show the peaks of both NR and CNCs. For example, the peaks of CNCs around 1624 cm^{-1} appear in the spectra of the NR/CNCs composites. There is no obvious shift of the peaks of the two components in the composites' spectra, suggesting no special interactions between them.

Figure 7b shows the XRD patterns of NR/CNCs composites. It can be seen that the pure NR exhibits a wide diffraction peak at 2θ = 20°, which indicates that the rubber matrix is in an amorphous state. The XRD patterns of CNCs show strong diffraction peaks of 2θ at 9.6°, 19.5°, 21°, 23°, and 26°, which are attributed to the (020), (110,040), (101), (130), and (013) planes, respectively.[20] When the content of CNCs in the composite is less than 5 wt %, no characteristic peaks of CNCs can be identified in the XRD patterns of the rubber composites owing to the small amount of CNCs. When the content of CNCs is beyond 5 wt %, the composites gradually show diffraction peaks of CNCs in the corresponding location especially at 9.6°. This suggests that the crystal structure of CNCs is not destroyed during processing of the composite. Hence, XRD results show that a different content of CNCs is successfully incorporated into the NR matrix.

To study the dispersion state of CNCs in the rubber matrix, examination of the cryofractured surface of composites was conducted using SEM. As shown in Figure 8, the cross section of the NR rubber is quite clear and smooth. In contrast, white spots appear in the SEM image of NR/CNCs composites, which represent the CNCs in the rubber composite. With increasing loading of CNCs, more and more CNCs can be

DOI: 10.1021/acssuschemeng.7b02586
ACS Sustainable Chem. Eng. 2018, 6, 325−336

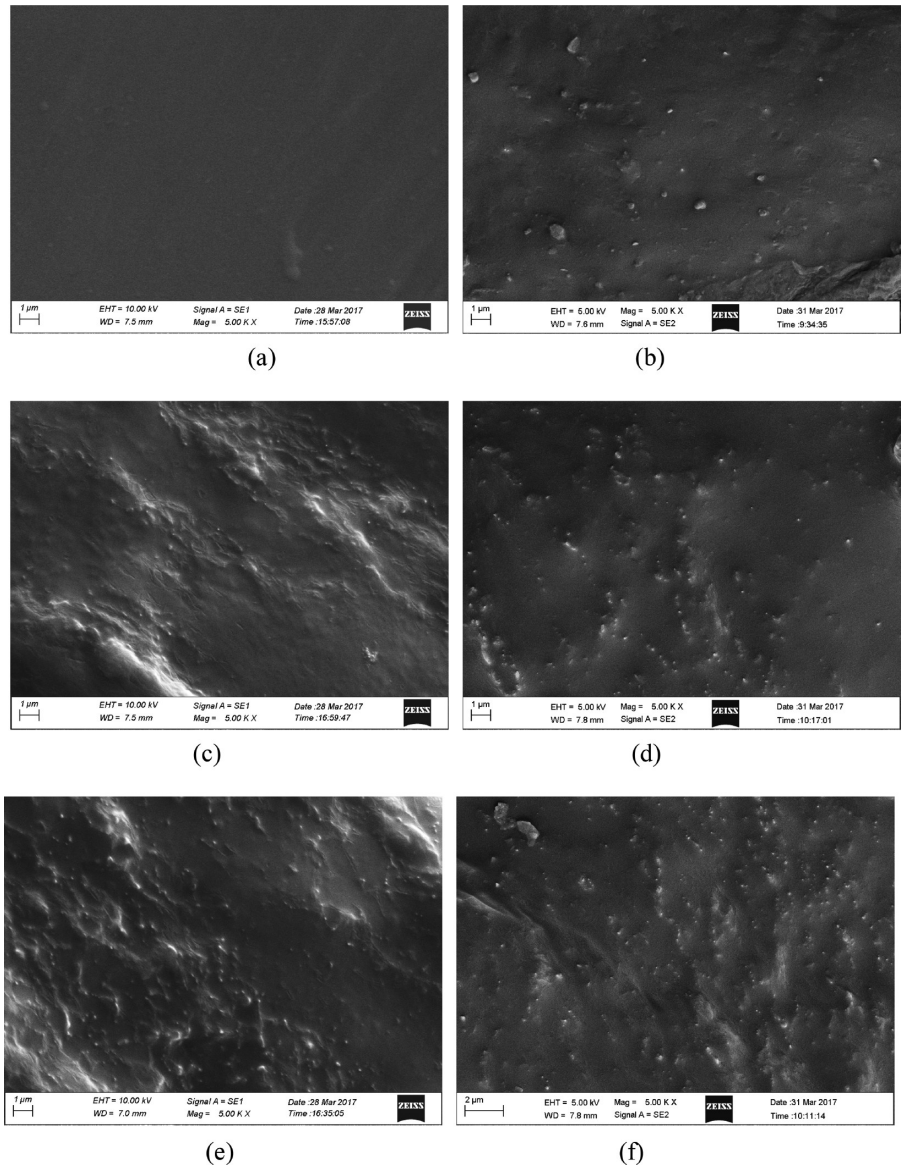

Figure 8. SEM images of NR/CNCs composites: (a) NR; (b) 1%; (c) 2.5%; (d) 5%; (e) 7.5%; (f) 10%.

observed in the matrix. Uniformly dispersed CNCs are observed within the rubber matrix, and nearly no aggregates of CNCs can be found. After carefully checking the images, one can see the interfaces of CNCs and the rubber are blurry, which suggests the good interfacial bonding in the composite. The FTIR, XRD, and SEM results demonstrate that CNCs are successfully incorporated into the NR matrix and can be dispersed evenly within the rubber. The high dispersibility of CNCs in other polymers such as polyacrylamide and carboxylated styrene butadiene rubber is also found.[8,20]

Mechanical Properties of the NR/CNCs Composites. CNCs with high aspect ratios and high strength (about 7.5 GPa of tensile strength) can be uniformly dispersed in the NR as seen from the SEM images above. Figure 9a shows the typical tensile stress−strain curves of NR/CNCs composite. The data of the mechanical properties are summarized in Table 1. The tensile strength of the NR/CNCs composites significantly increases with the addition of CNCs. For instance, the tensile strength of the composite with 10 wt % CNCs is 5.75 MPa, which is 6.25 times the pure NR. When the content of CNCs in the composites is less than 1 wt %, both the tensile strength and the elongation at break are improved simultaneously. With further increasing CNCs loading beyond 2.5 wt %, the tensile strength of the NR/CNCs composite continues to increase while the elongation at break starts to decrease. A rigid CNCs network can be formed in the rubber matrix with relatively high CNCs loading due to the interactions among the CNCs by electrostatic interaction and hydrogen bonding during the drying of the composite films.[49,56,57] It is expected that positively charged CNCs nanocrystals have repulsive electrostatic forces among them.[49] Also, chitin contains two kinds of hydrogen bonding linked with the C═O group, namely, intermolecular hydrogen bonding and the combination of intermolecular and intramolecular hydrogen bonding.[58] The intermolecular hydrogen bonds are NH···O═C and C(6)═OH···OH═C(6), while the intramolecular hydrogen bonds are C(3)═OH···O═C(5) and C(6)═OH···O═C. The rigid CNCs network can stiffen the composites by restricting the flexibility of rubber chains, resulting in the decrease in elongation at break.[40] From Table 1 the modulus at 100%,

DOI: 10.1021/acssuschemeng.7b02586
ACS Sustainable Chem. Eng. 2018, 6, 325−336

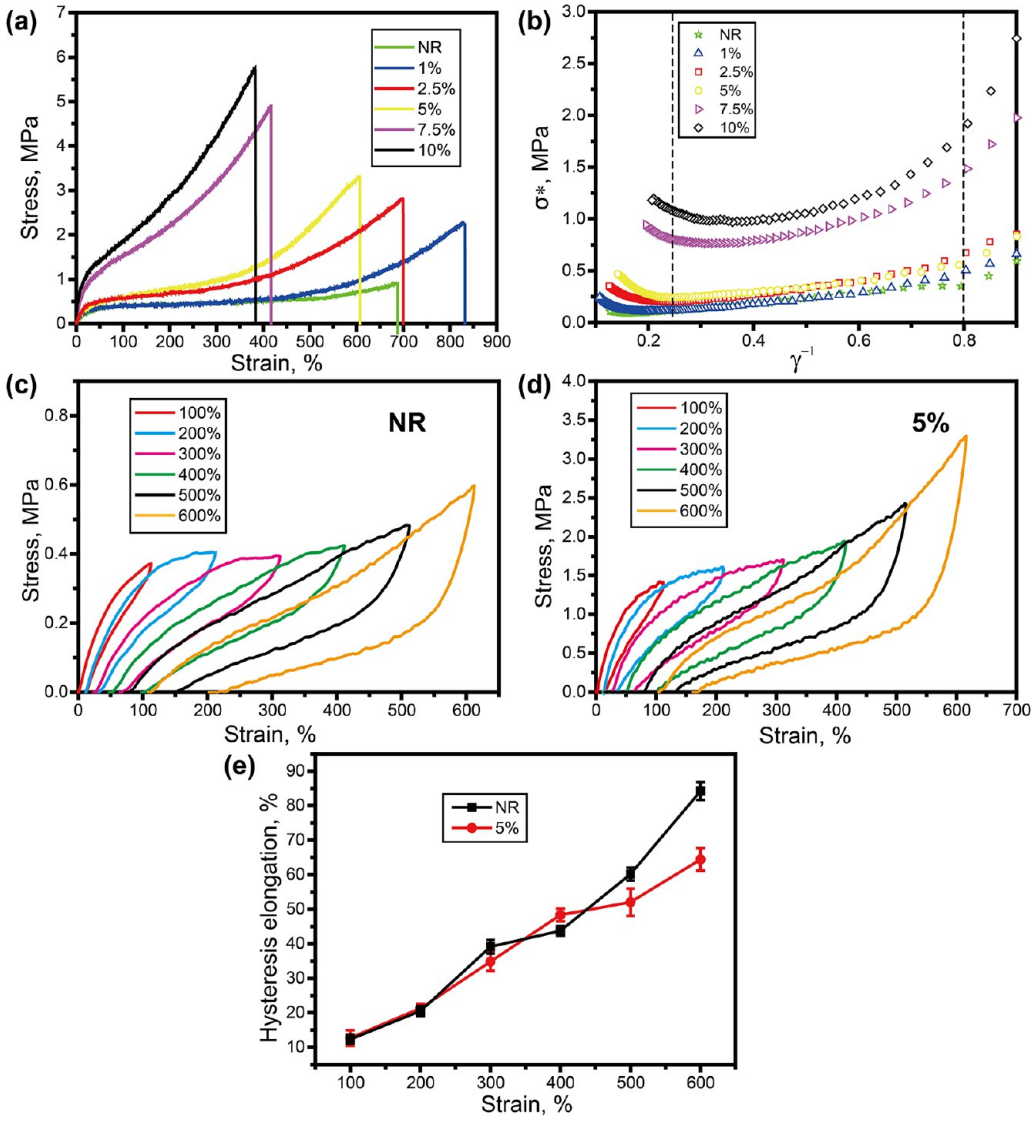

Figure 9. Tensile stress–strain curves of NR/CNCs composites (a); relationship between σ^* and λ^{-1} of NR/CNCs composites based on the Mooney–Rivlin equation (b); stress–strain curves of NR during successive tensile tests (c); stress–strain curves of 5% during successive tensile tests (d); hysteresis in elongations obtained from each cycle during successive tensile tests (e).

Table 1. Mechanical Properties of NR/CNCs Composite[a]

CNCs content (%)	modulus at 100% strain (MPa)	modulus at 300% strain (MPa)	modulus at 500% strain (MPa)	tensile strength (MPa)	elongation at break (%)	tear strength (kN/m)
0	0.40(0.07)	0.49(0.03)	0.56(0.04)	0.92(0.12)	685.1(28.0)	2.27(0.11)
1	0.40(0.09)	0.47(0.07)	0.68(0.10)	2.26(0.18)	825.8(36.5)	4.93(0.19)
2.5	0.57(0.03)	0.81(0.05)	1.47(0.08)	2.82(0.14)	699.2(20.8)	6.05(0.08)
5	0.59(0.10)	0.96(0.14)	2.17(0.11)	3.30(0.21)	606.7(30.0)	6.91(0.22)
7.5	1.53(0.04)	3.14(0.07)		4.90(0.15)	416.2(22.0)	9.89(0.23)
10	1.83(0.06)	4.20(0.10)		5.75(0.14)	382.6(24.6)	12.33(0.27)

[a]Data in parentheses represent standard deviation.

300%, and 500% strain (tensile stress at corresponding strain, similarly hereinafter) of the composites is also gradually increased with the increase of CNCs content (expect the tensile modulus at 100% and 300% for 1 wt % CNCs content). For example, the modulus at 500% strain of NR/CNCs composite with 5 wt % CNCs content is 2.17 MPa, which are 3.88 times the pure NR. Apart from tensile strength, the tear strength of the composites also obviously increases with the addition of CNCs. For example, the tear strength of composites with 10% CNCs content is 12.33 kN/m, which are 5.43 times the neat NR. The enhancement of mechanical performance can be attributed to the uniform dispersion of the CNCs and the structural character of CNCs.

To better illustrate the change of mechanical properties of the NR/CNCs composite, the tensile stress–strain data are recast using the Mooney–Rivlin equation.[59] The equation is given as follows

DOI: 10.1021/acssuschemeng.7b02586
ACS Sustainable Chem. Eng. 2018, 6, 325–336

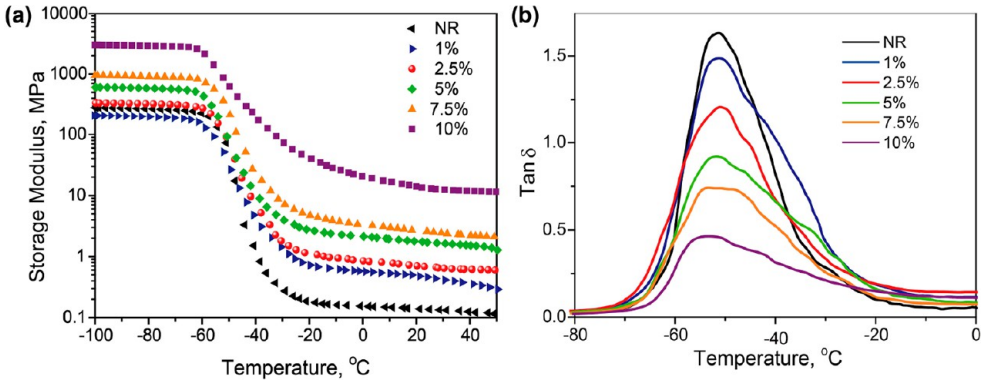

Figure 10. Temperature dependence of the storage modulus (E') of NR/CNCs composites with various CNCs contents (a); temperature dependence of the loss tangent (tan δ) of NR/CNCs composites with various CNCs contents (b).

$$\sigma^* = \sigma/(\lambda - \lambda^{-2}) \quad (3)$$

where σ^* is a reduced stress, σ is the true stress, and λ is the extension ratio which can be calculated by $\lambda = L/L_0 = 1 + \varepsilon$ (L and L_0 are the final and initial lengths, and ε is the tensile strain). As shown in Figure 9b, the Mooneye–Rivlin plots are divided into three sectors according to the strain: low strain ($1/\lambda > 0.8$), intermediate strain ($1/\lambda = \sim 0.25–0.8$), and high strain ($1/\lambda < 0.25$). The σ^* of neat NR is almost constant, while the σ^* of NR/CNCs composite increases with the CNCs loading. The increased σ^* is attributed to the limited extensibility of rubber chains bridged by adjacent particles upon stretching. A similar increasing trend of σ^* was also reported in other rubber/nanoparticle composites.[59,60] Figure 9c and 9d shows successive tensile hysteresis loops of NR and 5% NR/CNCs composite, respectively. It can be seen that both NR and composites can tolerate the six cyclic tests up to 600%. At the same strain the stress of the composite is much greater than that of NR. The hysteresis is compared in Figure 9e. Both NR and composite show increased hysteresis with the increase in the tensile strains. For example, the hysteresis of NR in the first cycle and the last cycle are 12.3% and 84.3%, respectively. Thus, it can be concluded that the elastic recovery of both NR and NR/CNCs composites is good upon small strain. The recovered strain is 230% for the NR after stretching to 600%, while the recovered strain of 5 wt % NR/CNCs composite is 168%. The hysteresis is less at high strain compared with that of NR due to the presence of the CNCs network, which suggests the addition of CNCs can increase the elastic recovery of the rubber via acting as physical cross-linking points.[61]

The formation of a liquid crystal of CNCs in dispersion is responsible for the formation of network structure in rubber matrix when preparing composites. The rigid CNCs network gives rise to the enhancement of the mechanical performance of the rubber composites. For comparison, we also added CNCs powder directly to NR by mechanical mixing on a two-roll open mill. It is found that CNCs cannot be evenly dispersed in rubber, and some large agglomerates emerge in the rubber matrix. The improvement in mechanical performance of NR is very marginal (data not shown). Therefore, the formation of CNCs liquid crystal structure contributes to the enhancement of the mechanical properties of the NR/CNCs composites.

The effect of CNCs on the dynamic properties of NR was further investigated by DMA. The storage modulus (E') and loss tangent (tan δ) of NR/CNCs composites are plotted as a function of temperature (Figure 10). It is shown that all materials exhibit a glassy–rubbery state transition in the temperature range from −100 to 50 °C. Table 2 summarizes the values of E' at −100, −40, and 30 °C and peak values and

Table 2. Data of Storage Modulus at Different Temperature, tan δ Peak Value, and tan δ Peak Temperature for NR/CNCs Composites

CNCs content (%)	storage modulus at −100 °C (MPa)	storage modulus at −40 °C (MPa)	storage modulus at 30 °C (MPa)	tan δ peak values (−)	tan δ peak temperature (°C)
0	279.40	1.20	0.13	1.64	−51.01
1	206.36	4.79	0.42	1.49	−51.01
2.5	340.54	7.69	0.64	1.209	−51.29
5	602.68	12.13	1.65	0.92	−51.90
7.5	946.44	22.71	2.44	0.74	−53.04
10	2992.68	218.01	12.48	0.46	−53.23

tan δ peak corresponding to the temperature of NR/CNCs composites. Also, E' of NR/CNCs composites increases with the CNCs loading (except the composite with 1% CNCs at glassy state) compared with that of pure NR. For example, the storage modulus at 30 °C of NR/CNCs composites at 10 wt % CNCs loading is 12.48 MPa, which is 96 times that of pure NR. The reinforcement effects illustrate that CNCs networks can effectively transfer load from the rubber matrix to the rigid nanoparticles. The slightly decreased E' in the rubber composite with 1% CNCs at glassy state is possibly related to the change in the conformation and free volume of the rubber by addition of a small amount of CNCs.[62]

The temperature at the maximum of the tan δ curve was designated as T_g. The T_g of NR/CNCs composites determined by DMA ranges from −51.0 to −53.2 °C. T_g shows a slightly decreased tendency with the CNCs loading. It has also been found in a previous study that the addition of nanofiller into rubber led to a decrease in T_g.[63] Peak values of the tan δ curve of the NR composites decrease with the CNCs loading. For instance, the peak value of the NR composite with 10% CNCs is 0.46, while that of neat NR is 1.64. The decrease is mainly owing to the reduction in polymer ratio in the NR/CNCs composites. In addition, the surfaces of CNCs can adsorb and restrict the mobility of rubber chains.[64] The interfacial interaction is strong in the NR/CNCs composites due to the high dispersibility of the CNCs, and CNCs play the role of physical cross-linking points to promote rubber chains entanglement. These are the reasons for the high reinforcement

DOI: 10.1021/acssuschemeng.7b02586
ACS Sustainable Chem. Eng. 2018, 6, 325–336

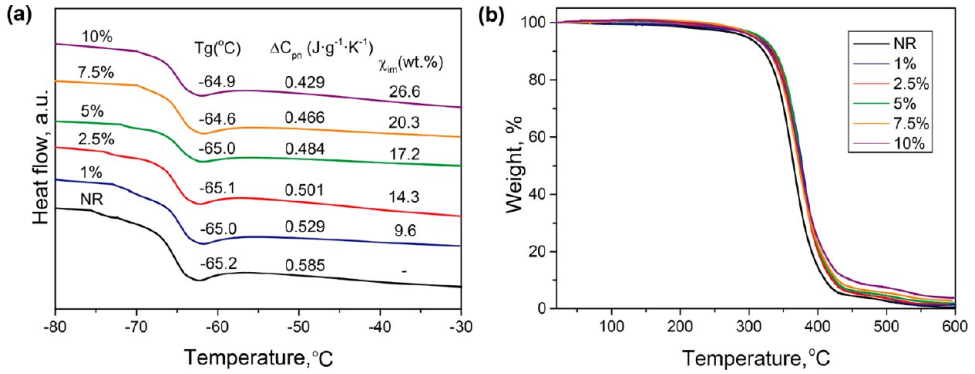

Figure 11. DSC heating curves of NR/CNCs composites with various CNCs contents (a); TGA curves of NR/CNCs composites with various CNCs contents (b).

effect of CNCs on NR. The decreased tan δ peak agrees with previously reported CNCs-reinforced rubber composites.[18]

Thermal Properties of NR/CNCs Composites. Figure 11a compares DSC heating curves of neat NR and NR/CNCs composites. All T_gs are located around −65 °C, and the addition of CNCs has no significant effect on the T_g of rubber. The T_g determined by DSC is ∼14 °C lower than that determined by DMA. This arises from the different principle for determining T_g for the two methods. The T_g determined by DMA highly relies on the test frequency,[65] while the DSC method measures the enthalpy change during heating or cooling.[20] To evaluate the amount of immobilized rubber around the CNCs in the composite, the value of χ_{im} (the mass percent of the immobilized polymer layer) was calculated from DSC data. Compared to pure NR, ΔC_{pn} (value of the heat capacity step) shows a systematic decreasing trend with increasing CNCs content. This suggests that more rubber molecular chains are confined between filler galleries in the NR/CNCs composites, and the confined rubber chains do not participate in the glass transition of the polymer bulk. When the content of filler increases, the value of χ_{im} gradually increases from 9.6% to 26.6%, suggesting a strong CNCs−rubber interfacial interaction.

The thermal stability of the NR/CNCs composites was further examined by TGA (Figure 11b). The weight loss curve of neat NR in the whole temperature range is well below the curves of NR/CNCs composites. This suggests that the thermal stability of NR increases by incorporation of CNCs. As discussed above, CNCs can restrict the mobility of rubber chains, and strong interfacial interactions are present in the NR/CNCs composites.[65] The residue at 600 °C of NR/CNCs composites increases with CNCs, which suggests CNCs are successfully incorporated into NR.

CONCLUSIONS

The liquid crystal behavior of CNCs dispersions is confirmed by polarized light microscopy. The liquid crystal phase begins to appear at a concentration of 5 wt %. The CNCs dispersion droplets with a concentration of 10 wt % retain the initial interference color pattern in the silicone oil via the self-assembly process. The organization of the CNCs into an ordered structure is critical for forming macroassembled CNCs architecture with tuned structure and ordered morphology. The rheological properties testing demonstrates sol−gel transition behavior upon increasing CNCs concentration. NR/CNCs composites are prepared by the solution-casting method. FTIR and XRD confirm that CNCs are successfully included into the NR matrix. SEM shows that CNCs are evenly distributed in the rubber matrix with good interface bonding. The tensile and tear tests suggest that CNCs can enhance the mechanical strength and modulus of NR significantly, while CNCs at a relatively high loading cause a decrease in the elongation at break. DMA shows that the storage modulus of NR composites increases with CNCs loading. The incorporation of CNCs can increase the thermal stability of NR/CNCs composites, which is attributed to the interfacial interaction-induced restriction of the rubber chains mobility. All results suggest that CNCs can improve both the mechanical property and the thermal stability of the rubber composites. The prepared NR/CNCs composites show potential applications in light color, lightweight, and high-performance rubber composites.

AUTHOR INFORMATION

Corresponding Author

*Tel/Fax: +86-20-8522 3271. E-mail: liumx@jnu.edu.cn.

ORCID

Mingxian Liu: 0000-0002-5466-3024

Author Contributions

The manuscript was written through the contributions of all authors. All authors have given approval to the final version of the manuscript.

Notes

The authors declare no competing financial interest.

ACKNOWLEDGMENTS

This work was financially supported by National Natural Science Foundation of China (51473069 and 51502113), the Guangdong Natural Science Funds for Distinguished Young Scholar (S2013050014606), the Guangdong Special support program (2014TQ01C127), the Science and Technology Planning Project of Guangdong Province (2014A020217006), the Pearl River S&T Nova Program of Guangzhou (201610010026), and the Science and Technology Program of Guangzhou, China (2017010160233 and 201510010135).

REFERENCES

(1) Ravi Kumar, M. N. A Review of Chitin and Chitosan Applications. *React. Funct. Polym.* **2000**, *46* (1), 1−27.

(2) Tomihata, K.; Ikada, Y. In Vitro and in Vivo Degradation of Films of Chitin and Its Deacetylated Derivatives. *Biomaterials* **1997**, *18* (7), 567−575.

DOI: 10.1021/acssuschemeng.7b02586
ACS Sustainable Chem. Eng. 2018, 6, 325−336

(3) Jayakumar, R.; Menon, D.; Manzoor, K.; Nair, S.; Tamura, H. Biomedical Applications of Chitin and Chitosan Based Nanomaterials—a Short Review. *Carbohydr. Polym.* **2010**, *82* (2), 227−232.
(4) Jayakumar, R.; Prabaharan, M.; Sudheesh Kumar, P. T.; Nair, S.; Tamura, H. Biomaterials Based on Chitin and Chitosan in Wound Dressing Applications. *Biotechnol. Adv.* **2011**, *29* (3), 322−337.
(5) Perrin, E.; Bizot, H.; Cathala, B.; Capron, I. Chitin Nanocrystals for Pickering High Internal Phase Emulsions. *Biomacromolecules* **2014**, *15* (10), 3766−3771.
(6) Mathew, A. P.; Laborie, M.-P. G.; Oksman, K. Cross-Linked Chitosan/Chitin Crystal Nanocomposites with Improved Permeation Selectivity and Ph Stability. *Biomacromolecules* **2009**, *10* (6), 1627−1632.
(7) Zeng, J.-B.; He, Y.-S.; Li, S.-L.; Wang, Y.-Z. Chitin Whiskers: An Overview. *Biomacromolecules* **2012**, *13* (1), 1−11.
(8) Liu, M.; Huang, J.; Luo, B.; Zhou, C. Tough and Highly Stretchable Polyacrylamide Nanocomposite Hydrogels with Chitin Nanocrystals. *Int. J. Biol. Macromol.* **2015**, *78*, 23−31.
(9) Huang, Y.; Yao, M.; Zheng, X.; Liang, X.; Su, X.; Zhang, Y.; Lu, A.; Zhang, L. Effects of Chitin Whiskers on Physical Properties and Osteoblast Culture of Alginate Based Nanocomposite Hydrogels. *Biomacromolecules* **2015**, *16* (11), 3499−3507.
(10) Wang, Q.; Chen, S.; Chen, D. Preparation and Characterization of Chitosan Based Injectable Hydrogels Enhanced by Chitin Nano-Whiskers. *J. Mech. Behav. Biomed. Mater.* **2017**, *65*, 466−477.
(11) Liu, L.; Wang, R.; Yu, J.; Jiang, J.; Zheng, K.; Hu, L.; Wang, Z.; Fan, Y. Robust Self-Standing Chitin Nanofiber/Nanowhisker Hydrogels with Designed Surface Charges and Ultralow Mass Content Via Gas Phase Coagulation. *Biomacromolecules* **2016**, *17* (11), 3773−3781.
(12) Sahraee, S.; Milani, J. M.; Ghanbarzadeh, B.; Hamishehkar, H. Physicochemical and Antifungal Properties of Bio-Nanocomposite Film Based on Gelatin-Chitin Nanoparticles. *Int. J. Biol. Macromol.* **2017**, *97*, 373−381.
(13) Sahraee, S.; Ghanbarzadeh, B.; Milani, J. M.; Hamishehkar, H. Development of Gelatin Bionanocomposite Films Containing Chitin and Zno Nanoparticles. *Food Bioprocess Technol.* **2017**, *10*, 1441−1453.
(14) Li, C.; Liu, H.; Luo, B.; Wen, W.; He, L.; Liu, M.; Zhou, C. Nanocomposites of Poly (L-Lactide) and Surface-Modified Chitin Whiskers with Improved Mechanical Properties and Cytocompatibility. *Eur. Polym. J.* **2016**, *81*, 266−283.
(15) Zou, Z.; Luo, C.; Luo, B.; Wen, W.; Liu, M.; Zhou, C. Synergistic Reinforcing and Toughening of Poly (L-Lactide) Composites with Surface-Modified Mgo and Chitin Whiskers. *Compos. Sci. Technol.* **2016**, *133*, 128−135.
(16) Liu, H.; Liu, W.; Luo, B.; Wen, W.; Liu, M.; Wang, X.; Zhou, C. Electrospun Composite Nanofiber Membrane of Poly (L-Lactide) and Surface Grafted Chitin Whiskers: Fabrication, Mechanical Properties and Cytocompatibility. *Carbohydr. Polym.* **2016**, *147*, 216−225.
(17) Gopalan Nair, K.; Dufresne, A. Crab Shell Chitin Whisker Reinforced Natural Rubber Nanocomposites. 1. Processing and Swelling Behavior. *Biomacromolecules* **2003**, *4* (3), 657−665.
(18) Gopalan Nair, K.; Dufresne, A. Crab Shell Chitin Whisker Reinforced Natural Rubber Nanocomposites. 2. Mechanical Behavior. *Biomacromolecules* **2003**, *4* (3), 666−674.
(19) Gopalan Nair, K.; Dufresne, A.; Gandini, A.; Belgacem, M. N. Crab Shell Chitin Whiskers Reinforced Natural Rubber Nanocomposites. 3. Effect of Chemical Modification of Chitin Whiskers. *Biomacromolecules* **2003**, *4* (6), 1835−1842.
(20) Liu, M.; Peng, Q.; Luo, B.; Zhou, C. The Improvement of Mechanical Performance and Water-Response of Carboxylated Sbr by Chitin Nanocrystals. *Eur. Polym. J.* **2015**, *68*, 190−206.
(21) Ma, L.; Liu, M.; Peng, Q.; Liu, Y.; Luo, B.; Zhou, C. Crosslinked Carboxylated Sbr Composites Reinforced with Chitin Nanocrystals. *J. Polym. Res.* **2016**, *23* (7), 1−11.
(22) Wu, X.; Lu, C.; Zhang, X.; Zhou, Z. Conductive Natural Rubber/Carbon Black Nanocomposites Via Cellulose Nanowhisker Templated Assembly: Tailored Hierarchical Structure Leading to Synergistic Property Enhancements. *J. Mater. Chem. A* **2015**, *3* (25), 13317−13323.
(23) Zhang, X.; Wu, X.; Lu, C.; Zhou, Z. Dialysis-Free and in Situ Doping Synthesis of Polypyrrole@ Cellulose Nanowhiskers Nanohybrid for Preparation of Conductive Nanocomposites with Enhanced Properties. *ACS Sustainable Chem. Eng.* **2015**, *3* (4), 675−682.
(24) Cao, J.; Lu, C.; Zhuang, J.; Liu, M.; Zhang, X.; Yu, Y.; Tao, Q. Multiple Hydrogen Bonding Enables the Self-Healing of Sensors for Human-Machine Interaction. *Angew. Chem., Int. Ed.* **2017**, *56* (30), 8795−8800.
(25) Kelnar, I.; Kovářová, J.; Tishchenko, G.; Kaprálková, L.; Pavlová, E.; Carezzi, F.; Morganti, P. Chitosan/Chitin Nanowhiskers Composites: Effect of Plasticisers on the Mechanical Behaviour. *J. Polym. Res.* **2015**, *22* (2), 5.
(26) Yan, W.; Shen, L.; Ji, Y.; Yang, Q.; Shen, X., Chitin Nanocrystal Reinforced Wet-Spun Chitosan Fibers. *J. Appl. Polym. Sci.* **2014**, *131*(19) 10.1002/app.40852.
(27) Liu, M.; Zheng, H.; Chen, J.; Li, S.; Huang, J.; Zhou, C. Chitosan-Chitin Nanocrystal Composite Scaffolds for Tissue Engineering. *Carbohydr. Polym.* **2016**, *152*, 832−840.
(28) Baltzer, D. H. Liquid Crystal Systems. *Google Patents*, 1971.
(29) Habibi, Y.; Lucia, L. A.; Rojas, O. J. Cellulose Nanocrystals: Chemistry, Self-Assembly, and Applications. *Chem. Rev.* **2010**, *110* (6), 3479−3500.
(30) Parker, R. M.; Frka-Petesic, B.; Guidetti, G.; Kamita, G.; Consani, G.; Abell, C.; Vignolini, S. Hierarchical Self-Assembly of Cellulose Nanocrystals in a Confined Geometry. *ACS Nano* **2016**, *10* (9), 8443−8449.
(31) Luo, Z.; Song, H.; Feng, X.; Run, M.; Cui, H.; Wu, L.; Gao, J.; Wang, Z. Liquid Crystalline Phase Behavior and Sol−Gel Transition in Aqueous Halloysite Nanotube Dispersions. *Langmuir* **2013**, *29* (40), 12358−12366.
(32) Behabtu, N.; Lomeda, J. R.; Green, M. J.; Higginbotham, A. L.; Sinitskii, A.; Kosynkin, D. V.; Tsentalovich, D.; Parra-Vasquez, A. N. G.; Schmidt, J.; Kesselman, E. Spontaneous High-Concentration Dispersions and Liquid Crystals of Graphene. *Nat. Nanotechnol.* **2010**, *5* (6), 406−411.
(33) Xu, Z.; Gao, C. Aqueous Liquid Crystals of Graphene Oxide. *ACS Nano* **2011**, *5* (4), 2908−2915.
(34) Werbowyj, R. S.; Gray, D. G. Ordered Phase Formation in Concentrated Hydroxypropylcellulose Solutions. *Macromolecules* **1980**, *13* (1), 69−73.
(35) Shimamura, K.; White, J. L.; Fellers, J. F. Hydroxypropylcellulose, a Thermotropic Liquid Crystal: Characteristics and Structure Development in Continuous Extrusion and Melt Spinning. *J. Appl. Polym. Sci.* **1981**, *26* (7), 2165−2180.
(36) Dreyfuss, P.; Gent, A. N.; Williams, J. R. Tear strength and tensile strength of model filled elastomers. *J. Polym. Sci., Polym. Phys. Ed.* **1980**, *18* (10), 2135−2142. Maiti, M.; Paramguru, R. Stress distribution due to an external crack opened by two rigid inclusions. *Eng. Fract. Mech.* **1980**, *13* (4), 767−773.
(37) Revol, J.-F.; Marchessault, R. In Vitro Chiral Nematic Ordering of Chitin Crystallites. *Int. J. Biol. Macromol.* **1993**, *15* (6), 329−335.
(38) Platé, N. A. f. *Liquid-Crystal Polymers*; Springer Science & Business Media, 2013.
(39) Alonso, B.; Belamie, E. Chitin−Silica Nanocomposites by Self-Assembly. *Angew. Chem., Int. Ed.* **2010**, *49* (44), 8201−8204.
(40) Li, J.; Revol, J.; Naranjo, E.; Marchessault, R. Effect of Electrostatic Interaction on Phase Separation Behaviour of Chitin Crystallite Suspensions. *Int. J. Biol. Macromol.* **1996**, *18* (3), 177−187.
(41) Tzoumaki, M. V.; Moschakis, T.; Biliaderis, C. G. Metastability of Nematic Gels Made of Aqueous Chitin Nanocrystal Dispersions. *Biomacromolecules* **2010**, *11* (1), 175−181.
(42) Nguyen, T. D.; Shopsowitz, K. E.; MacLachlan, M. J. Mesoporous Silica and Organosilica Films Templated by Nanocrystalline Chitin. *Chem. - Eur. J.* **2013**, *19* (45), 15148−15154.
(43) Nguyen, T. D.; MacLachlan, M. J. Biomimetic Chiral Nematic Mesoporous Materials from Crab Cuticles. *Adv. Opt. Mater.* **2014**, *2* (11), 1031−1037.

DOI: 10.1021/acssuschemeng.7b02586
ACS Sustainable Chem. Eng. 2018, 6, 325−336

(44) Nguyen, T.-D.; Shopsowitz, K. E.; MacLachlan, M. J. Mesoporous Nitrogen-Doped Carbon from Nanocrystalline Chitin Assemblies. *J. Mater. Chem. A* **2014**, *2* (16), 5915−5921.
(45) Lee, C. G.; Da Silva, C. A.; Dela Cruz, C. S.; Ahangari, F.; Ma, B.; Kang, M.-J.; He, C.-H.; Takyar, S.; Elias, J. A. Role of Chitin and Chitinase/Chitinase-Like Proteins in Inflammation, Tissue Remodeling, and Injury. *Annu. Rev. Physiol.* **2011**, *73*, 479−501.
(46) Muzzarelli, R. A.; Boudrant, J.; Meyer, D.; Manno, N.; DeMarchis, M.; Paoletti, M. G. Current Views on Fungal Chitin/Chitosan, Human Chitinases, Food Preservation, Glucans, Pectins and Inulin: A Tribute to Henri Braconnot, Precursor of the Carbohydrate Polymers Science, on the Chitin Bicentennial. *Carbohydr. Polym.* **2012**, *87* (2), 995−1012.
(47) Zhong, C.; Cooper, A.; Kapetanovic, A.; Fang, Z.; Zhang, M.; Rolandi, M. A Facile Bottom-up Route to Self-Assembled Biogenic Chitin Nanofibers. *Soft Matter* **2010**, *6* (21), 5298−5301.
(48) Fan, Y.; Fukuzumi, H.; Saito, T.; Isogai, A. Comparative Characterization of Aqueous Dispersions and Cast Films of Different Chitin Nanowhiskers/Nanofibers. *Int. J. Biol. Macromol.* **2012**, *50* (1), 69−76.
(49) Tzoumaki, M. V.; Moschakis, T.; Biliaderis, C. G. Metastability of Nematic Gels Made of Aqueous Chitin Nanocrystal Dispersions. *Biomacromolecules* **2010**, *11* (1), 175−181.
(50) Zhao, X.; Xu, Z.; Xie, Y.; Zheng, B.; Kou, L.; Gao, C. Polyelectrolyte-Stabilized Graphene Oxide Liquid Crystals against Salt, Ph, and Serum. *Langmuir* **2014**, *30* (13), 3715−3722.
(51) Gabriel, J.-C. P.; Sanchez, C.; Davidson, P. Observation of Nematic Liquid-Crystal Textures in Aqueous Gels of Smectite Clays. *J. Phys. Chem.* **1996**, *100* (26), 11139−11143.
(52) Li, J.; Revol, J.; Marchessault, R. Rheological Properties of Aqueous Suspensions of Chitin Crystallites. *J. Colloid Interface Sci.* **1996**, *183* (2), 365−373.
(53) Van de Velde, K.; Kiekens, P. Structure Analysis and Degree of Substitution of Chitin, Chitosan and Dibutyrylchitin by Ft-Ir Spectroscopy and Solid State 13 C Nmr. *Carbohydr. Polym.* **2004**, *58* (4), 409−416.
(54) Salomon, G.; Van Der Schee, A. C. Infrared Analysis of Isomerized, Vulcanized and Oxidized Natural Rubber. *J. Polym. Sci.* **1954**, *14* (74), 181−192.
(55) Tripathy, A. R.; Morin, J. E.; Williams, D. E.; Eyles, S. J.; Farris, R. J. A Novel Approach to Improving the Mechanical Properties in Recycled Vulcanized Natural Rubber and Its Mechanism. *Macromolecules* **2002**, *35* (12), 4616−4627.
(56) Lu, Y.; Weng, L.; Zhang, L. Morphology and Properties of Soy Protein Isolate Thermoplastics Reinforced with Chitin Whiskers. *Biomacromolecules* **2004**, *5* (3), 1046−1051.
(57) Watthanaphanit, A.; Supaphol, P.; Tamura, H.; Tokura, S.; Rujiravanit, R. Fabrication, Structure, and Properties of Chitin Whisker-Reinforced Alginate Nanocomposite Fibers. *J. Appl. Polym. Sci.* **2008**, *110* (2), 890−899.
(58) Kameda, T.; Miyazawa, M.; Ono, H.; Yoshida, M. Hydrogen Bonding Structure and Stability of A-Chitin Studied by 13c Solid-State Nmr. *Macromol. Biosci.* **2005**, *5* (2), 103−106.
(59) Peddini, S.; Bosnyak, C.; Henderson, N.; Ellison, C.; Paul, D. Nanocomposites from Styrene−Butadiene Rubber (SBR) and Multiwall Carbon Nanotubes (MWCNT) Part 2: Mechanical Properties. *Polymer* **2015**, *56*, 443−451.
(60) Jia, Z.-x.; Luo, Y.-f.; Yang, S.-y.; Guo, B.-c.; Du, M.-l.; Jia, D. -m., Morphology, Interfacial Interaction and Properties of Styrene-Butadiene Rubber/Modified Halloysite Nanotube Nanocomposites. *Chin. J. Polym. Sci.* **2009**, *27* (06), 857−864.
(61) Angellier, H.; Molina-Boisseau, S.; Dufresne, A. Mechanical Properties of Waxy Maize Starch Nanocrystal Reinforced Natural Rubber. *Macromolecules* **2005**, *38* (22), 9161−9170.
(62) Mackay, M. E.; Dao, T. T.; Tuteja, A.; Ho, D. L.; Van Horn, B.; Kim, H.-C.; Hawker, C. J. Nanoscale Effects Leading to Non-Einstein-Like Decrease in Viscosity. *Nat. Mater.* **2003**, *2* (11), 762.
(63) Mélé, P.; Marceau, S.; Brown, D.; de Puydt, Y.; Albérola, N. D. Reinforcement Effects in Fractal-Structure-Filled Rubber. *Polymer* **2002**, *43* (20), 5577−5586.
(64) Visakh, P.; Thomas, S.; Oksman, K.; Mathew, A. P. Crosslinked Natural Rubber Nanocomposites Reinforced with Cellulose Whiskers Isolated from Bamboo Waste: Processing and Mechanical/Thermal Properties. *Composites, Part A* **2012**, *43* (4), 735−741.
(65) Vadukumpully, S.; Paul, J.; Mahanta, N.; Valiyaveettil, S. Flexible Conductive Graphene/Poly (Vinyl Chloride) Composite Thin Films with High Mechanical Strength and Thermal Stability. *Carbon* **2011**, *49* (1), 198−205.

DOI: 10.1021/acssuschemeng.7b02586
ACS Sustainable Chem. Eng. 2018, 6, 325−336